ResearchGate

See discussions, stats, and author profiles for this publication at: https://www.researchgate.net/publication/23150515

Intracellular Delivery of Quantum Dot–Protein Cargos Mediated by Cell Penetrating Peptides

ARTICLE *in* BIOCONJUGATE CHEMISTRY · SEPTEMBER 2008

Impact Factor: 4.51 · DOI: 10.1021/bc800089r · Source: PubMed

CITATIONS
107

READS
24

7 AUTHORS, INCLUDING:

Thomas Pons
École Supérieure de Physique et de Chimie…
107 PUBLICATIONS **3,941** CITATIONS
SEE PROFILE

Hedi Mattoussi
Florida State University
202 PUBLICATIONS **21,802** CITATIONS
SEE PROFILE

Available from: Hedi Mattoussi
Retrieved on: 02 February 2016

Intracellular Delivery of Quantum Dot−Protein Cargos Mediated by Cell Penetrating Peptides

Igor L. Medintz,*,† Thomas Pons,‡,# James B. Delehanty,† Kimihiro Susumu,‡ Florence M. Brunel,§ Philip E. Dawson,§ and Hedi Mattoussi*,‡

Center for Bio/Molecular Science and Engineering, Code 6900, and Division of Optical Sciences, Code 5611, U.S. Naval Research Laboratory, Washington, DC 20375, and Departments of Cell Biology and Chemistry and the Skaggs Institute for Chemical Biology, The Scripps Research Institute, La Jolla, California 92037. Received March 5, 2008; Revised Manuscript Received June 19, 2008

We utilize cell penetrating peptide functionalized QDs as specific vectors for the intracellular delivery of model fluorescent protein cargos. Multiple copies of two structurally diverse fluorescent proteins, the 27 kDa monomeric yellow fluorescent protein and the 240 kDa multichromophore b-phycoerythrin complex, were attached to QDs using either metal-affinity driven self-assembly or biotin−Streptavidin binding, respectively. Cellular uptake of these complexes was found to depend on the additional presence of cell-penetrating peptides within the QD−protein conjugates. Once inside the cells, the QD conjugates were mostly distributed within endolysosomal compartments, indicating that intracellular delivery of both QD assemblies was primarily driven by endocytotic uptake. Cellular microinjection of QD-fluorescent protein assemblies was also utilized as an alternate delivery strategy that could bypass the endocytic pathway. Simultaneous signals from both the QDs and the fluorescent proteins allowed verification of their colocalization and conjugate integrity upon delivery inside live cells. Due to their intrinsic fluorescence properties, this class of proteins provides a unique tool to test the ability of QDs functionalized with cell penetrating peptides to mediate the intracellular delivery of both small and large size protein cargos. Use of QD−peptide/fluorescent protein vectors may make powerful tools for understanding the mechanisms of nanoparticle-mediated drug delivery.

INTRODUCTION

Developing nanoparticles as delivery vehicles for drugs, genes, and contrast/imaging agents to live cells, tissues, and tumors has stimulated much interest recently (*1*−*5*). Among an array of available nanoparticles, luminescent semiconductor nanocrystals or quantum dots (QDs) provide a powerful prototypical example with many demonstrated applications in biological imaging and sensing (*6*−*9*). Their utility is derived from the combination of unique photophysical characteristics and sizes comparable to that of a large protein. The hydrodynamic radius of hydrophilic CdSe-ZnS QDs varies from ∼5 nm, for nanocrystals cap exchanged with molecular ligands, to ∼20 nm for nanocrystals encapsulated within block copolymers (*10*). A single QD can be conjugated to several biomolecules (such as antibodies, peptides, DNA) to provide multifunctional QD bioconjugates with enhanced avidity. In addition, their strong resistance to chemical and photodegradation can potentially allow long-term fluorescent monitoring of specific biological processes (*6*−*9, 11*).

Several methods have been investigated to achieve the efficient intracellular delivery of various nanoparticles, including QDs. They include electroporation (*12*), lipid-based transfection reagents (*13, 14*), and microinjection (*13*), as well as receptor-mediated endocytosis (*11, 15*). Use of cell-penetrating peptides (CPP) conjugated to hydrophilic QDs as an alternate strategy to facilitate their intracellular uptake has also been reported by several groups, and results suggest that delivery was primarily driven by endocytotic uptake (*13, 16*−*23*). Although a wide range of cell penetrating peptides exist, they are most often functional analogues of the canonical HIV-derived TAT sequence and usually consist of 8−10 sequentially repeated polyarginine residues (*24*). We have recently explored the use of CPP-mediated delivery of QD−peptide conjugates to eukaryotic HEK-293 and COS-1 cells (*25*). The peptide sequence used was modular and consisted of a C-terminal 8 arginine repeat-block for mediating cellular uptake, a short linker/spacer, and a N-terminal 8 histidine tract that promoted peptide self-assembly onto CdSe-ZnS core−shell QDs (*25, 26*). Efficiency of the CPP-facilitated delivery was found to depend on both peptide-to-QD ratio and overall QD conjugate concentration. CPP-mediated uptake required short incubation times of less than 1 h compared to 2−4 h or longer incubation time for passive uptake; it was also both selective and specific even when cells were incubated with mixtures of CPP and *other* nonpeptide functionalized QDs. Nanocrystals delivered via this approach did not exhibit any discernible toxic effects to the cells, and intracellular localization was again confirmed to be primarily endosomal (*25*). The intracellular delivery and stability of nanocrystals conjugated to a mixture of His-terminated CPP and dye-labeled peptides was further verified by multiphoton fluorescence resonance energy transfer imaging (FRET between QDs and proximal dyes) of intracellular compartments several hours post-uptake (*27*).

In this report, we build upon our previous results and demonstrate that cell penetrating peptides can further promote the effective intracellular delivery of QD cargos made of

* Email: hedi.mattoussi@nrl.navy.mil; igor.medintz@nrl.navy.mil.
† Center for Bio/Molecular Science and Engineering, Code 6900, U.S. Naval Research Laboratory.
‡ Division of Optical Sciences, Code 5611, U.S. Naval Research Laboratory.
§ The Scripps Research Institute.
# Present address: Institut National de la Santé et de la Recherche Médicale, Laboratoire Photons et Matière, CNRS UPRA0005, ESPCI, 10 Rue Vauquelin, 75005 Paris, France.

10.1021/bc800089r CCC: $40.75 © 2008 American Chemical Society
Published on Web 08/06/2008

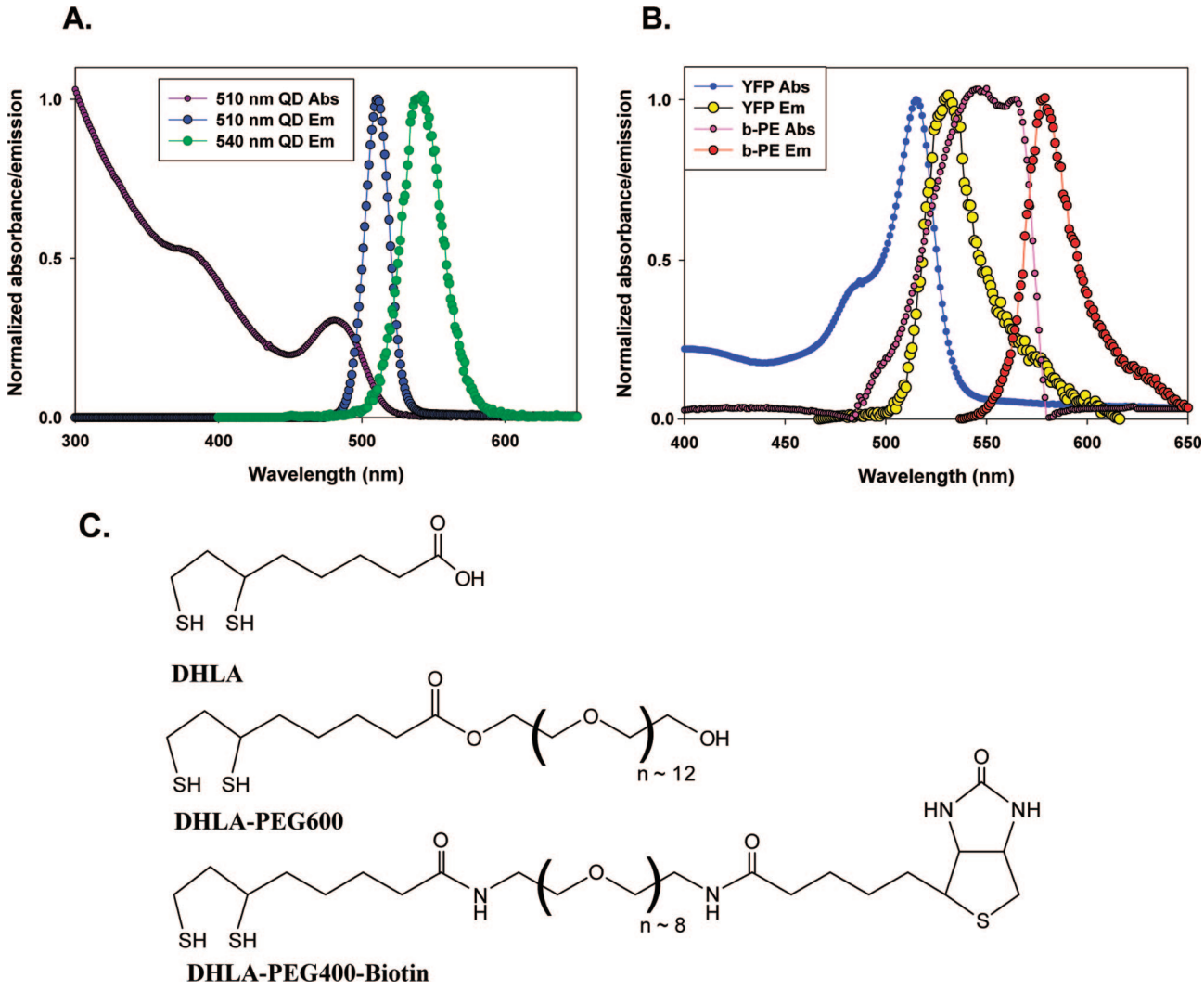

Figure 1. Absorption and emission spectra of QDs and fluorescent proteins used. (A) Normalized absorption spectrum of 510 nm emitting QDs along with the normalized PL spectra of 510 and 540 nm emitting QDs. (B) Normalized absorption and emission spectra of yellow fluorescent protein (YFP) and b-phycoerythrin (b-PE). (C) Structure of the DHLA, DHLA-PEG600, and DHLA-PEG400-biotin ligands used to provide aqueous compatibility of the QDs.

nanocrystals self-assembled with additional small or large fluorescent proteins. The QD serves as a central nanoscaffold for immobilizing proteins and peptides, while the CPPs promote conjugate internalization by eukaryotic cells. This class of proteins was specifically selected as they allow fluorescence monitoring of intracellular distribution as well as testing of the stability of QD−protein assemblies. Proteins, including yellow fluorescent protein (YFP) and the multichromophore b-phycoerythrin complex (b-PE), were conjugated to QDs, via a combination of metal-affinity interactions and biotin−avidin binding. We found that intracellular delivery of these conjugates strongly depended on CPP presence, while colocalization studies indicated that the mixed surface QD−peptide/protein assemblies were distributed within the endosomal compartments. In comparison, direct microinjection of QD−protein cargos into live cells bypassed the endolysosomal system and resulted in more homogeneous distribution of conjugates throughout the cytosol.

EXPERIMENTAL PROCEDURES

QD Synthesis. CdSe-ZnS core−shell QDs with emission maxima centered at 510 and 540 nm were synthesized using stepwise reactions of organometallic precursors in hot coordinating solvent mixtures following the procedures described in refs (*28*−*31*); absorption and emission spectra are provided in Figure 1A. The nanocrystals were made hydrophilic by exchanging the native capping shell, composed primarily of trioctyl phosphine and trioctyl phosphine oxide (TOP/TOPO), with bifunctional ligands as described in refs (*32*−*34*). We used two sets of hydrophilic QDs: (1) nanocrystals capped with only dihydrolipoic acid, and (2) nanocrystals capped with a mixture of poly(ethylene glycol)-appended dihydrolipoic acid (PEG Mw ≃ 600, DHLA-PEG) and biotin-terminated DHLA-poly(ethylene glycol) (PEG Mw ≃ 400, DHLA-PEG-biotin) with a 9:1 molar ratio of the ligands; these are referred to as DHLA-QDs and DHLA-PEG-biotin-QDs, respectively. Ligand structures are provided in Figure 1C (*32*−*34*).

Proteins and Peptides. The yellow fluorescent protein was generously provided by W. Frommer (Carnegie Institute, Stanford, CA) on plasmid pRSET B (Invitrogen, Carlsbad, CA) within a gene fusion encoding a blue fluorescent protein−glucose binding protein−yellow fluorescent protein sensor construct inserted between *Bam*HI and *Hind*III of the multiple cloning site (*35*). The blue fluorescent protein−glucose binding protein portion was excised by digestion with *Kpn*I and *Bam*HI and an insert encoding for a hexa-histidine $(His)_6$ sequence followed by a unique *Xho*I site (Asp-Gln) was ligated into the *Kpn*I and *Bam*HI restriction sites. Transformants were screened by *Xho*I digestion and confirmed with DNA sequencing. The final YFP

gene construct sequentially encodes a His_6 sequence after the start methionine, Asp-Gln, an Xpress Epitope (Asp-Leu-Tyr-Asp-Asp-Asp-Asp-Lys) and another His_6 sequence at the immediate N-terminus of the YFP coding sequence. This plasmid was introduced into BL21(DE3) *E. coli* cells (Invitrogen) and expression induced with 1 mM isopropyl-β-D-thiogalactopyranoside (IPTG, Sigma, St Louis, MO) for 3 days at 30 °C in the dark to allow for full maturation of the chromophore, before harvesting the cells by centrifugation at 4 °C. His-appended YFP was purified from soluble cell lysate using Ni-NTA Resin (Qiagen, Valencia, CA), as described in refs (*35, 36*). The absorption and emission spectra of the purified YFP are shown in Figure 1B. One-to-one b-phycoerythrin−Streptavidin conjugate solution at 1 mg/mL (referred to as b-PE) and AlexaFluor 647 dye-labeled Transferrin (AF647-TF, $\lambda_{abs\ max.} = 647$ nm, $\lambda_{em\ max.} = 670$ nm) were obtained from Invitrogen. Cell penetrating peptide (CPP) with the sequence $(His)_8$-Trp-Leu-Ala-Aib-Ser-Gly-$(Arg)_8$-amide, where Aib is α-aminoisobutyric acid and the c-terminus is blocked with an amide, was synthesized and purified as described in ref (*25*).

Self-Assembly of Quantum Dot Bioconjugates. To self-assemble QD−YFP conjugates at the desired valence, His-appended proteins at the appropriate molar ratios were added to 0.3 μM of 510-nm emitting DHLA-capped QDs in 10 mM Tris-Cl pH 8 buffer and incubated at room temp for ∼30 min. Similarly, b-PE-Streptavidin was added to 0.3 μM of 540-nm emitting QDs (capped with DHLA-PEG:DHLA-PEG-biotin 9:1 ratio) in phosphate buffered saline (137 mM NaCl, 10 mM phosphate, 2.7 mM KCl, pH 7.4, PBS) and incubated at 4 °C overnight; conjugate formation in this case is driven by Streptavidin−biotin interactions. Conjugates were characterized using gel electrophoresis, where changes in the electrophoretic mobility of QDs assembled with either His-appended YFP or Streptavidin-labeled b-PE were monitored (*10*). Samples were diluted in 1 × TBE buffer (0.09 M Tris, 0.002 M Na_2-EDTA 0.09 M Boric acid pH ∼8.3) and run on 1% or 2% agarose gels for QD−b-PE and YFP conjugates, respectively. In particular, the effects of varying the number of proteins per QD bioconjugate were monitored. Gel images were collected by exciting the QD and/or protein and capturing fluorescence images of the separated bands within the gels using a Kodak 440 Digital Image Station (Rochester, NY). Conjugate formation was also confirmed by monitoring changes in the energy transfer between the QDs and fluorescent proteins upon self-assembly. Fluorescent spectra were collected on a Tecan Safire Dual Monochromator Multifunction Microtiter Plate Reader (Tecan, Research Triangle Park, NC) using 325 nm excitation. For intracellular delivery and imaging experiments, QDs were self-assembled with a mixture of the protein and CPP at a nominal CPP:QD molar ratio of 50:1.

Intracellular Uptake of Quantum Dot−Fluorescent Protein Conjugates. HEK 293T/17 and COS-1 cell lines (ATCC, Manassas, VA) were cultured in complete growth medium (Dulbecco's Modified Eagle's Medium (DMEM) supplemented with 4 mM L-glutamine, 1 mM sodium pyruvate, 1% (v/v) penicillin/streptomycin/actinomycin D antibiotic/antimycotic, and 10% (v/v) heat-inactivated fetal bovine serum (FBS). Cells were incubated at 37 °C under 5% CO_2 atmosphere and a subculture was performed every 3 days (*25*). Cellular internalization experiments were performed in sterile Laboratory-Tek chambered coverglass wells (Nunc, Rochester, NY). The chambers were initially coated with 50 μg/mL fibronectin (Sigma-Aldrich, St Louis, MO) in sodium bicarbonate buffer pH 8.5. Approximately 2×10^4 cells were seeded into the wells and cultured overnight. QD bioconjugates were diluted into complete culture medium and added to the cell culture and incubated at 37 °C for 1 h. AF647-TF (at 40 μg/mL) was also added to the culture to specifically colabel the endosomal vesicles as described previously (*25*). Mixed surface QD conjugates consisting of either 1:5 or 1:10 QD/YFP and QD/b-PE with assembly valence of 1:1 to 1:2.5, together with CPP at ∼50 CPPs per QD, were incubated with the cell cultures at different QD conjugate concentrations. Excess unbound QD conjugates were removed by washing the culture at least 3 times with PBS. Cells were then fixed in 3.7% paraformaldehyde for 10 min at room temperature, washed twice with PBS, and mounted in ProLong Antifade mounting media containing DAPI dye (Invitrogen) for nuclear staining. Epifluorescence image collection was carried out using an Olympus IX-71 microscope. Side-by-side split fluorescence images were collected and quantitated using a DualView system (Optical Insights, Tucson, AZ) equipped with a 565 nm dichroic filter. For 510 nm QD−YFP cellular imaging, samples were excited at 488 nm and emissions were collected/separated with the 565 nm dichroic and deconvoluted. QD fluorescence was collected at $\lambda < 565$ nm and the YFP fluorescent tail collected at $\lambda > 565$ nm. YFP leakage into the QD window was subtracted as part of the deconvolution. The 540 nm QDs and b-PE were excited at 488 nm and their respective emissions were separated with the 565 nm dichroic filter and deconvoluted. DAPI fluorescence was excited using a Xe lamp and emission collected using a DAPI cube (D350/50× for excitation, dichroic 400DCLP, D460/50m for detection). AF647-TF was excited using the Xe lamp and fluorescence detected using a Cy5 cube (excitation HQ620/60×, dichroic Q660LP, emission HQ700/75m). Both excitation/detection cubes were provided by Chroma Technology (Rockingham, VT). Differential interference contrast (DIC) images were collected using a bright light source. For microinjection, the QD−YFP and QD−b-PE conjugates described above were diluted in PBS. Conjugates were directly injected into adherent COS-1 or HEK 293T/17 cells using an InjectMan NI2 micromanipulator equipped with a FemtoJet programmable microinjector (Eppendorf, Westbury, NY). This instrumental setup allows the injection of femtoliter aliquots of conjugate solution into individual cells (*37*).

RESULTS

Fluorescent Proteins and Self-Assembly of Quantum Dot Bioconjugates. Yellow fluorescent protein (YFP) is a slightly longer wavelength emitting variant of the green fluorescent protein (GFP), and is derived from the jellyfish *Aequorea*, as described in the work of Tsien (*38*). It consists of 11 β-strands which form a hollow β-barrel or cylinder, and the chromophore, located at the center of a threaded helix, is formed by a cyclic rearrangement of three central residues (Gly_{65}, Tyr_{66}, Gly_{67}) during maturation (*38*). This relatively small protein (Mw ∼27 kDa) is easily expressed in bacteria from a plasmid, has a short maturation time, and has been used in a variety of FRET-based intracellular sensing studies (*39−41*). The second fluorescent protein we used, b-phycoerythrin (b-PE), is a member of the phycobiliprotein family of light harvesting protein complexes known as phycobilisomes found in red algae and cyanobacteria (*42, 43*). b-PE differs photophysically and structurally from YFP in many respects; see Table 1. It consists of α/β monomers associated into a symmetrical $(\alpha/\beta)_6$ hexameric structure and has ca. 34−38 covalently attached bilins (open chain tatrapyrrole chromophores) per functional moiety. It has a large molecular weight, ∼10 times that of YFP, a very large extinction coefficient, ∼100 times higher than that of YFP, and has been widely used as a highly sensitive fluorescent probe (*42, 43*).

We utilize two self-assembly approaches to form our QD bioconjugates: metal-affinity interactions and biotin−avidin binding. When used for nanoparticle conjugation, metal affinity

Table 1. Properties of the Fluorescent Protein Assemblies Tested[a]

protein	structure	molecular weight (kDa)	extinction coefficient (M^{-1} cm^{-1})	quantum yield (QY)	quantum dot	method of QD attachment
YFP	11-stranded β-barrel	~27 000	20 200	0.60	510 nm QDs (QY ~ 12%)	metal-affinity coordination
b-PE	multi-subunit multichromophore protein assembly	~240 000 Streptavidin ~64 000	2 410 000	0.98	540 nm QDs (QY ~ 19%)	biotin-streptavidin

[a] b-PE utilized as a 1:1 Streptavidin conjugate (*38, 42, 43*).

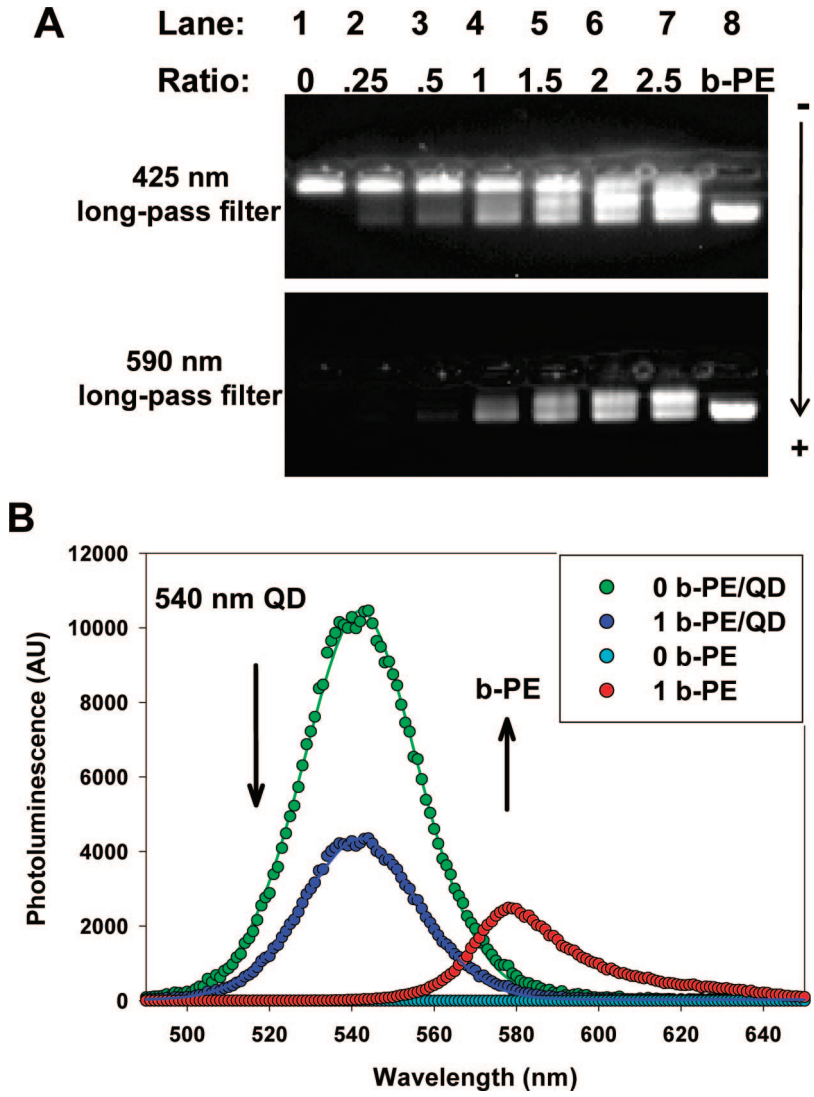

Figure 2. Agarose gel electrophoresis and FRET data. (A) Electrophoretic mobility bands captured from self-assembled QD−Streptavidin−b-PE conjugates; the corresponding average conjugate valences (ratio of b-PE per QD) are listed on top of each lane. Lane 8 has the equivalent amount of 2.5 b-PE alone. The gel was imaged with the indicated filters to isolate QD and protein emissions. QD−b-PE conjugates were separated on 1% agarose gels. (B) Deconvoluted PL spectra of 540 nm DHLA-PEG-biotin-QDs in the absence and presence of ~1 b-PE/QD along with b-PE FRET-sensitized emission. QD PL was fit to a Gaussian profile.

driven self-assembly can be versatile and easy to implement. We and other groups have shown that polyhistidine (His_n) sequences facilitate self-assembly of both proteins and peptides onto ZnS-overcoated CdSe QDs (*6, 44−46*). More recently, we elucidated the kinetics of metal-His driven self-assembly between QDs and both proteins and peptides and showed that high affinity/low dissociation constants drive the interactions ($K_D \sim 10^{-9}-10^{-8}$ M) (*26*). This study further showed that His interactions occur directly with the Zn-rich inorganic surface of the nanocrystals. Engineering YFP with an N-terminus bearing two-$(His)_6$ sequences separated by a small spacer and CPP having an N-terminal $(His)_8$ sequence permit the formation of tight QD−protein/peptide complexes driven by this self-assembly. Biotin−avidin binding is a ubiquitous bioconjugation strategy in biology, known for its strong interaction ($K_D \sim 10^{-15}$ M) (*47*). Using QDs surface-capped with a mixture of hydroxyl- and biotin-terminated PEG (DHLA-PEG-biotin-QDs) allowed easy conjugation to commercially available b-PE−Streptavidin.

The first characterization technique of these QD bioconjugates relied on agarose gel electrophoresis (no SDS present), where changes in the mobility shift were measured for QDs alone and QDs conjugated to increasing number of proteins. For QD−b-PE conjugates, since the emissions of the QDs and protein are spectrally distinguishable, gels were imaged with 425 and 590

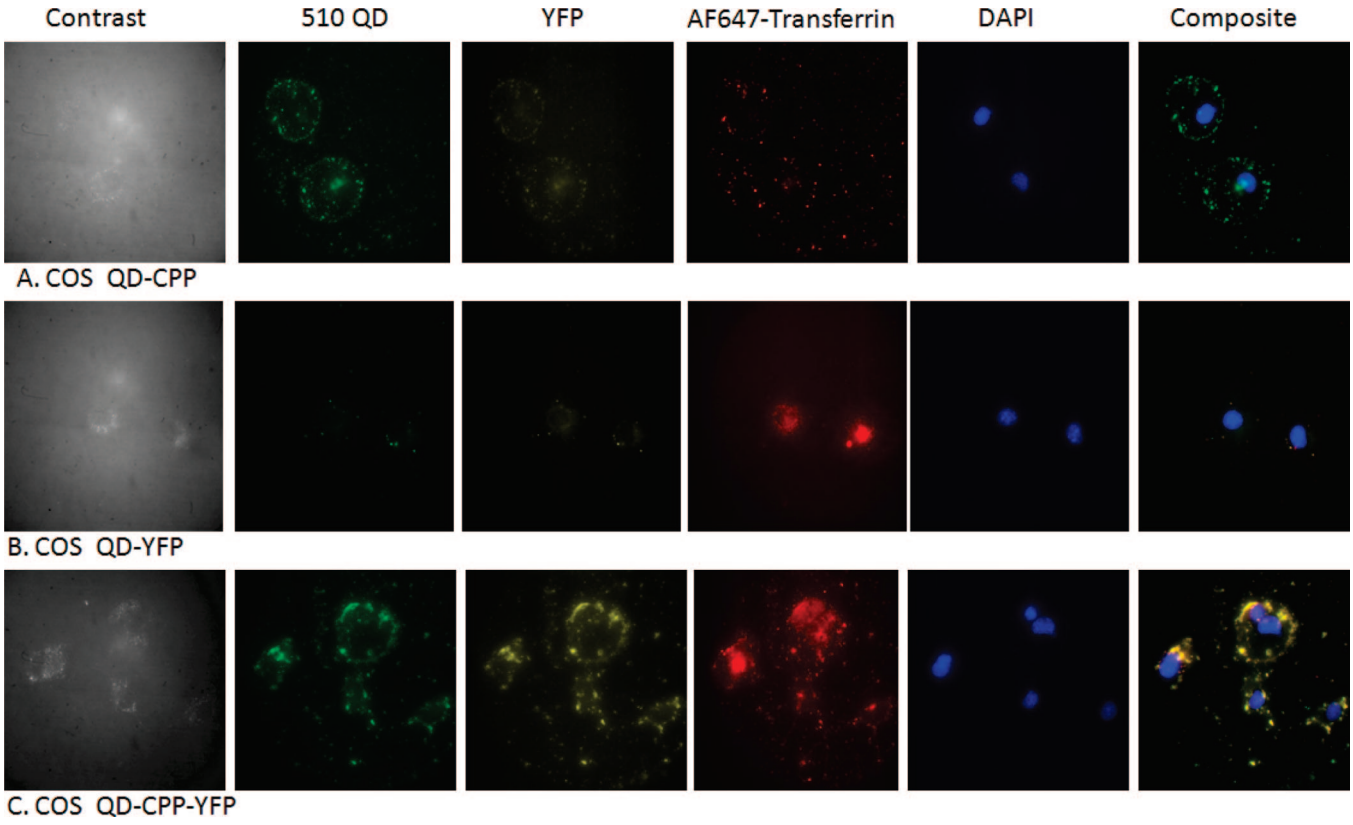

Figure 3. Cellular uptake of QD−YFP bioconjugates. Images collected from COS-1 cells incubated with (A) QD−CPP, (B) QD−YFP, and (C) QD−CPP−YFP assemblies; QD conjugate solutions at 75 nM concentration were used. For each series (left to right) the contrast, fluorescence images for 510-nm QD, YFP, AF647-Transferrin, DAPI, together with the merged fluorescence composite images are shown. Scale bar is 10 μm.

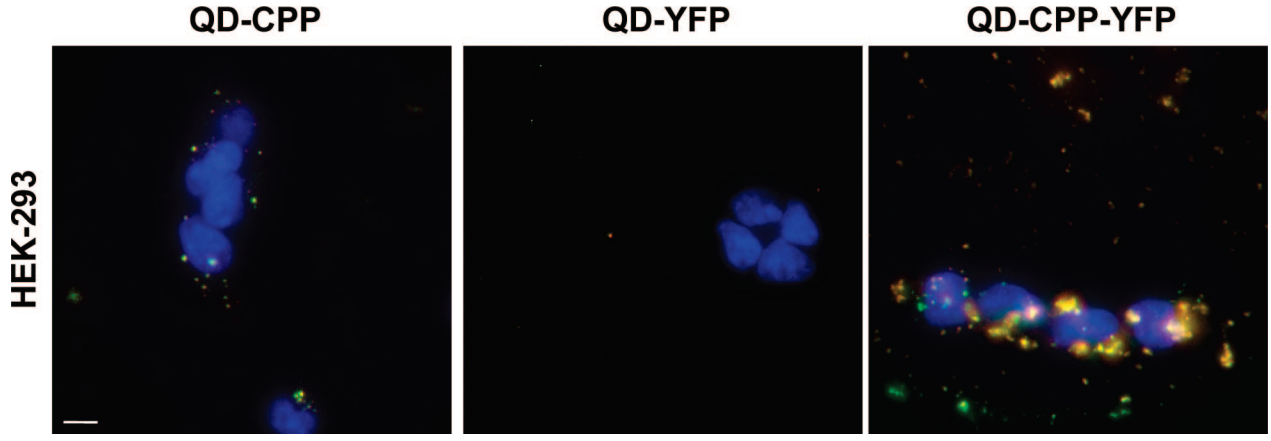

Figure 4. Cellular uptake of QD−YFP bioconjugates. HEK293/T17 cells were incubated with QD−CPP, QD−YFP, and CD−CPP−YFP assemblies as shown in Figure 2. Only merged representative fluorescent images compiled from the DAPI, QD, and YFP emissions are shown for each conjugate. Scale bar is 10 μm.

nm long-pass filters to allow visualization of either the simultaneous QD and b-PE emissions or only the emission of b-PE (see Figure 2A for representative images). The mobility of the unconjugated QDs capped with DHLA-PEG600/DHLA-PEG400-biotin mixture was essentially zero, as these ligands do not impart a net charge to the QDs. In comparison, a finite mobility shift was measured for b-PE alone. For solutions of conjugates at increasing b-PE-to-QD ratio, one can easily discern a discrete band with mobility intermediate between those of the QDs and b-PE (lanes 1 and 8, respectively). A concomitant decrease in the PL of the QD band is also noted as the ratio of b-PE and conjugate formation increases, which can be attributed to FRET interactions (see below). Furthermore, when the mobility bands corresponding to the various b-PE-to-QD ratios (lanes 2−7) and that of b-PE (control in lane 8) are compared, it appears that in addition to the main QD−b-PE conjugates, bands corresponding to the QDs and b-PE alone can also be visualized. The distribution in mobility bands for the conjugate solution is attributed to a distribution of conjugate valences varying between zero and the maximum expected, as previously observed for self-assembled bioconjugates (*10, 48*). The valence of QD conjugates is described by Poisson statistics and its effects are usually more visible at low protein-to-QD ratio as is the case in the present samples. Further, it is quite possible that not all the b-PE is conjugated to Streptavidin. Similarly, we carried out a side-by-side comparison of the mobility band shifts of solutions of QD−YFP conjugates at increasing YFP-to-QD ratios together with that of unconjugated QDs (data not shown).

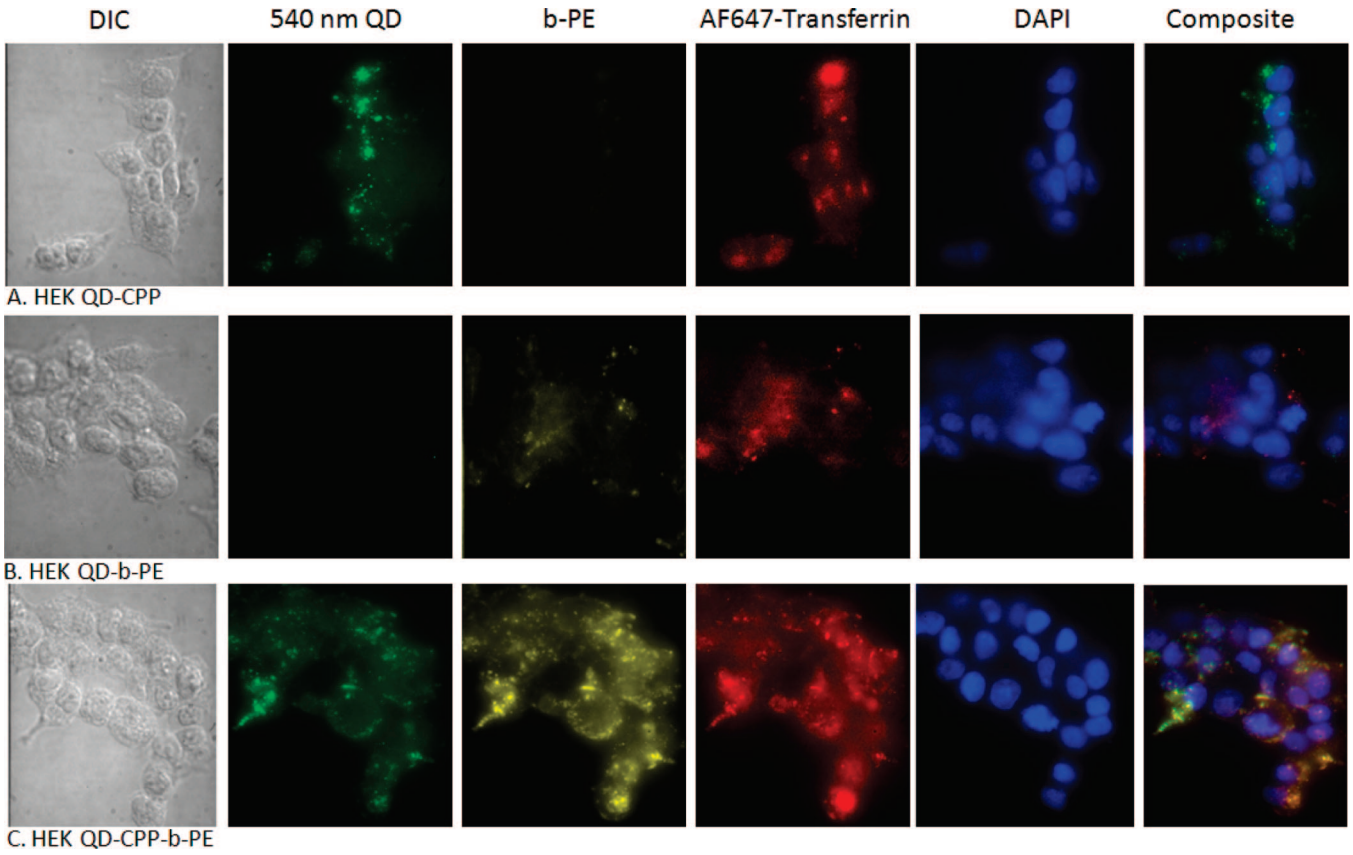

Figure 5. Cellular uptake of QD−b-phycoerythrin conjugates. Representative images of HEK293/T17 cells incubated with (A) QD−CPP, (B) QD−b-PE, (C) QD−CPP−b-PE. 540 nm emitting QD conjugates at 75 nM concentration were used. For each set of conjugates, the corresponding contrast, fluorescence images of 540-nm QD, b-PE, AF647-Transferrin, DAPI, along with the merged composite fluorescence images are shown. Due to overlap between the QD and b-PE emissions, spectral leakage between the QD and b-PE fluorescence can be seen along with some b-PE adherence to the cell membrane. Scale bar is 10 μm.

QDs exhibited the highest mobility shift due to the presence of negative surface charges (deprotonated carboxyl groups on the DHLA ligands), while a decrease in mobility shift with increasing conjugate valence was measured, which we attributed to an increase in conjugate size, i.e., YFP retards QD migration as more proteins are attached to the QD.

Assembly of both sets of QD−YFP and QD−b-PE conjugates were further confirmed by "visualizing" FRET between the central QD and proximal fluorescent proteins within the conjugates. The favorable spectral overlap between the nanocrystal emissions and either of the fluorescent proteins should result in a significant FRET interaction; see Figure 1. Representative deconvoluted spectra are shown in Figure 2B for QD−b-PE conjugates, where a loss in QD PL is measured along with a concomitant increase in acceptor PL upon conjugate, in agreement with previous results collected from solutions of QD−protein/peptide−dye conjugates (*10, 48−50*). Monitoring the relative QD donor and fluorescent protein acceptor emissions at different acceptor ratios allowed us to choose optimal assembly ratios for cellular uptake experiments. For imaging, significant emission from both the QD donor and the FRET-sensitized acceptor protein were desired. A detailed description and analysis of the FRET interactions will be presented elsewhere.

Intracellular Delivery of QD−YFP Conjugates. To verify that uptake of QDs surface functionalized with YFP cargo is mediated by the presence of CPP on the nanocrystal surface, two different cell lines, COS-1 and HEK293/T17, were separately incubated with 3 types of conjugate: QD−CPP conjugates (∼50 CPP per QD), QD−YFP conjugates (10 YFP per QD in the absence of CPP), and QDs assembled with a mixture of YFP and CPP (QD−YFP−CPP with ∼10 YFP and 50 CPP per conjugate). Cells were incubated with solutions of 510-nm emitting QD conjugates (at ∼75 nM concentration), rinsed to remove any unbound materials, and subsequently imaged using epifluorescence microscopy. Cells were also counter-stained with DAPI and AF647-transferrin to allow visualization of the nuclei and endosomes, respectively. Figure 3 shows images collected for COS-1 cells incubated with the indicated QD bioconjugates. Each row of panels shows representative DIC, 510-nm emitting QDs (green), YFP (yellow), AF647-TF (red), DAPI (blue), and the merged fluorescent composite images (right). Figure 4 shows only the merged images collected for the HEK cells similarly incubated with the three types of QD bioconjugates. The images collected for both types of cells indicate that in the absence of CPP there is essentially no intracellular uptake of QDs or QD−YFP conjugates during the incubation times used; the weak fluorescence measured in a few of the cells is attributed to nonspecific binding to the cell surfaces. When additional CPP is presented on the QD surface (mixed surface QD−protein−CPP conjugates), a substantial intracellular uptake of conjugates takes place as indicated by the pronounced fluorescence intensity measured for both sets of cells. Furthermore, images collected for both cultures showed that there is a nearly complete overlap between the fluorescence patterns of the QD and YFP; see last column of images in Figure 3 for COS-1 and merged images in Figure 4 for HEK293. Overlap between emissions of the QDs ($\lambda_{em} \sim 510$ nm) and YFP ($\lambda_{em} \sim 530$ nm) results in a small, non-negligible leakage of fluorescence signals between the respective images, as complete spectral separation is not possible with the dichroic filters used (see QD and YFP images in Figure 3). Evaluation of the staining patterns and colocalization with

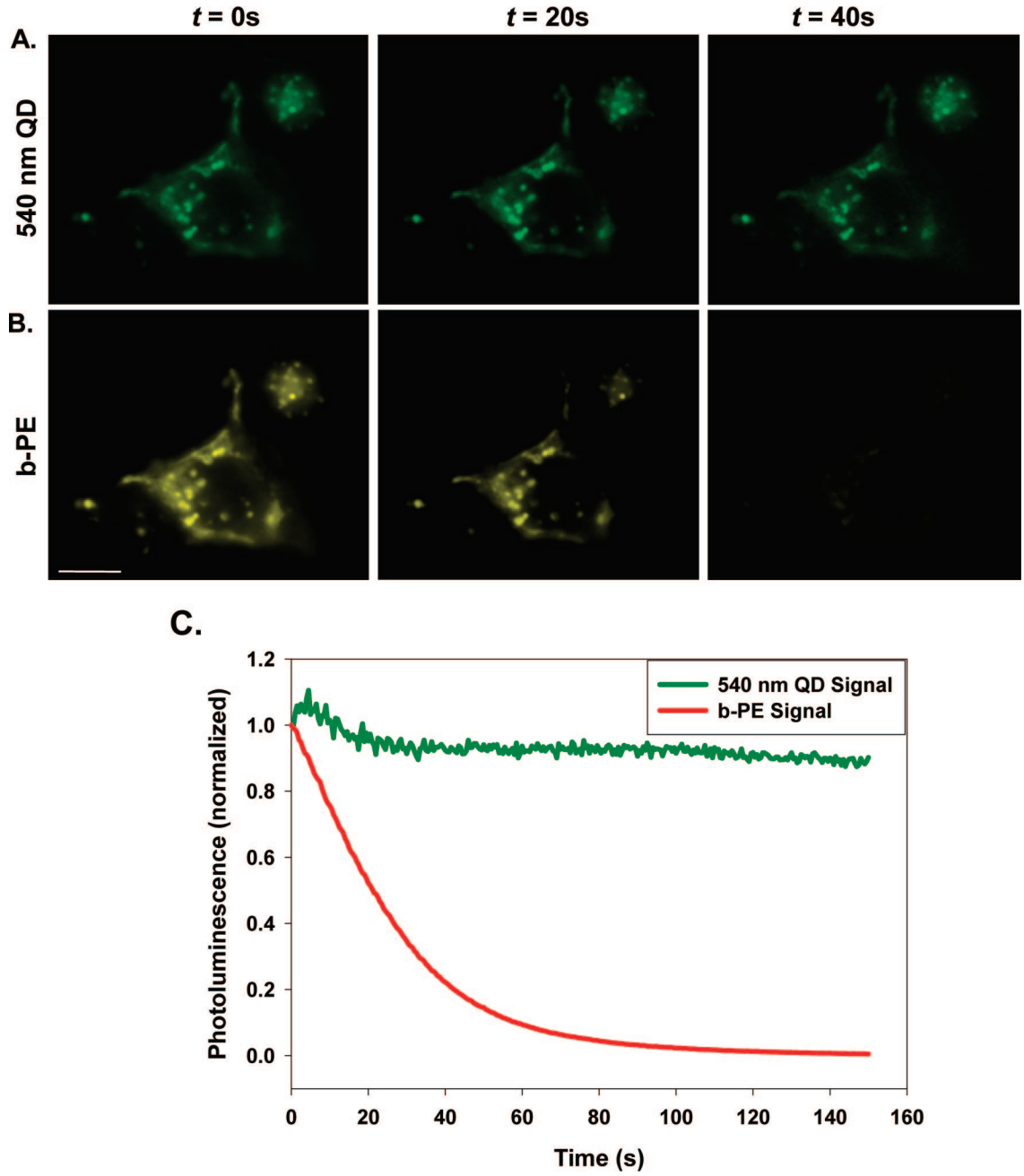

Figure 6. Photobleaching of intracellular QD−b-phycoerythrin conjugates. HEK293/T17 cells incubated with QD−CPP−b-PE conjugates and continuously illuminated with 488 nm laser excitation. (A) 540 nm QD and (B) b-PE fluorescence signals were separated using the Dualview imaging system and monitored over time; images shown were collected at the indicated time intervals. Scale bar is 10 μm. (C) Progression of integrated fluorescence intensity with time collected from the QD and protein emission channels.

the endosome-specific AF647-TF marker indicate that QD−protein/peptide conjugates remain intact after uptake, have a perinuclear distribution, and are predominantly confined within endosomal compartments. The efficient internalization of QD conjugates by both cell lines only in the presence of CPP again demonstrates that CPP facilitates the specific intracellular uptake of QDs surface-functionalized with fluorescent protein cargos and uptake is driven mainly by endocytosis. This result complements and supports our previous findings using QD−CPP conjugates, reported in ref (*25*).

Delivery of QD−b-Phycoerthrin Conjugates. Confident in the ability of CPP to promote the cellular uptake of QD bioconjugates carrying multiple copies of a relatively small protein, we next challenged this delivery mechanism with a far larger protein complex. Streptavidin conjugated b-PE (total estimated Mw ~300 kDa) were attached to DHLA-PEG-biotin-QDs with emission centered at 540 nm and, as done above, three variations of QD conjugates were incubated with HEK293/T17 cells: QD−CPP conjugates (no b-PE), QD−b-PE conjugates (no CPP), and QD−CPP−b-PE assemblies (protein and peptide both present). Average ratios of ~1 and 2.5 b-PE per QD conjugate were used. Each row of images displayed in Figure 5A−C shows representative DIC, 540 nm QD emission (green), b-PE (yellow), AF647-TF (red), DAPI (blue), and merged composite fluorescence images (right) for each of the three QD conjugates tested. Data are shown for QD−b-PE with valence of 1, but similar results were collected for conjugates having 2.5 b-PE per QD conjugate (not shown). As found above with YFP, CPP is the key mediator of cellular uptake. The strong fluorescence of b-PE is a clear reflection of the natural brightness of these proteins. The pattern of staining from the QD, b-PE, and Transferrin-marker channels in cells exposed to the

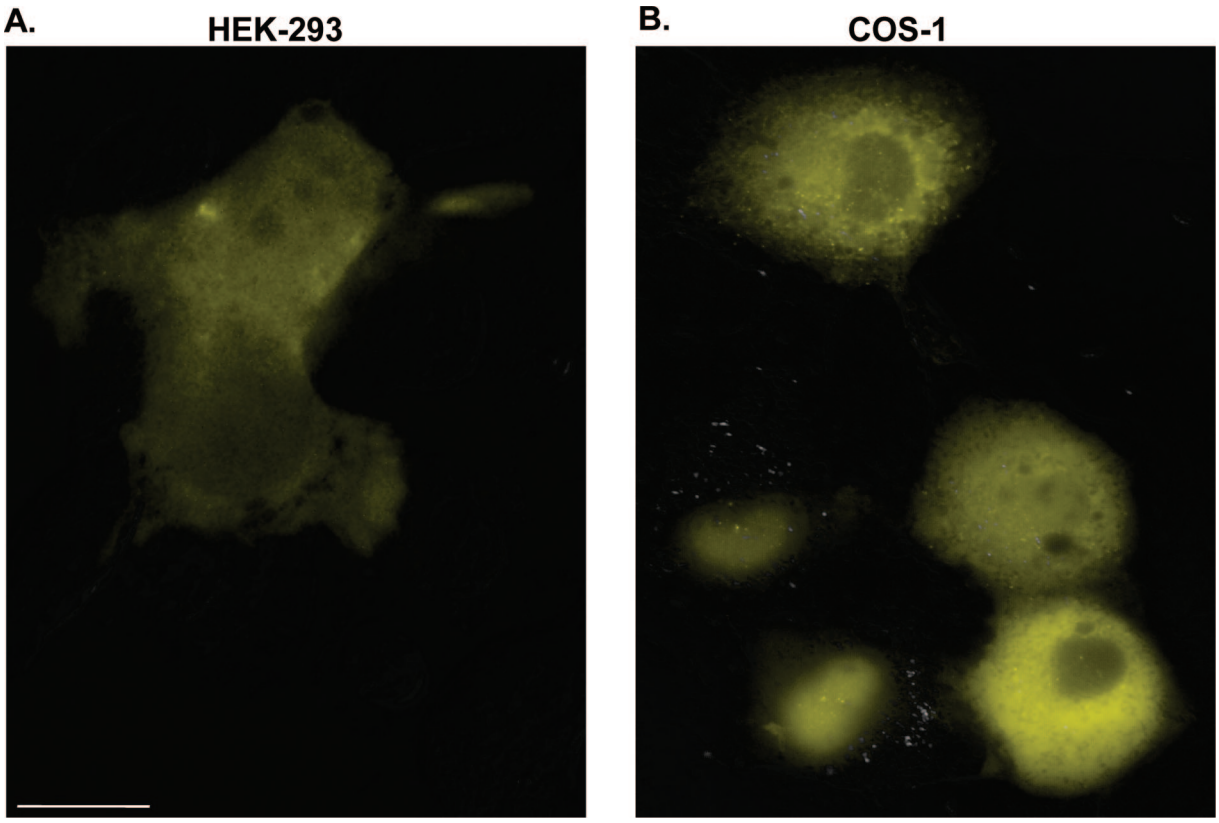

Figure 7. Cellular microinjection. 1:1 540 nm DHLA-PEG-biotin/QD−b-PE conjugates were microinjected directly into the cytosol of HEK293/T17 and COS-1 cells. Representative merged DIC and fluorescence images are shown. Note the clearly distinguishable nuclei in some of the COS-1 cells. Scale bar is 10 μm.

QD−CPP−b-PE assemblies are fully superimposable, which again strongly suggests that the b-PE remains attached to the nanocrystal and primarily localized within the endosomes. Similar results were also obtained with COS-1 cells (data not shown).

One of the unique features of luminescent QDs with direct relevance to biological imaging is their strong resistance to degradation combined with high photobleaching thresholds as compared to conventional dyes (*11, 51*). For example, Wu and co-workers compared the fluorescence decay of AlexaFluor 488 and CdSe-ZnS QDs in fixed 3T3 cells under continuous illumination and found that, while the dye fluorescence is essentially bleached after ~60 s, the QD signal persists for orders of magnitude longer exposure times (*51*). Our QD−YFP and QD−b-PE conjugates stay assembled after uptake and they thus offer an easy side-by-side comparison of QD and fluorescence protein signals for colocalization and stability studies. COS-1 cells incubated with 540 nm QD−CPP−b-PE bioconjugates were continuously excited at 488 nm for extended periods of time and the fluorescence signals of the QD and b-PE were separated using the DualView imaging system equipped with a 565 nm dichroic filter. The representative images shown in Figure 6A,B together with the plot of integrated PL intensities from each channel (Figure 6C) indicate that the b-PE signal decays to ~50% of its initial value in ca. 20 s and to less than 5% within 90 s. In comparison, the QD signal remains essentially unperturbed. The present comparison using fluorescent proteins extends and confirms prior findings on the pronounced QD resistance to photobleaching, using intracellular side-by-side comparisons between QDs and fluorescent dyes (*51*). This result also confirms the intracellular colocalization of the assembled conjugates, as the pattern of the rapidly bleached b-PE fluorescence is completely superimposed over the QD fluorescence pattern. Furthermore, by direct inference this also proves the structural and functional integrity of the QD−fluorescent protein cargos after delivery inside live cells.

DISCUSSION

Our results clearly show that cell-penetrating peptides can mediate the intracellular delivery of QDs conjugated to additional proteins of substantially larger size and molecular weight. This expands our previous results, where CPP was found to facilitate uptake of QD−CPP conjugates by eukaryotic cells (*25*). It also expands the findings by Torchilin and co-workers, where TAT peptide on the surface of liposomes allowed their intracellular delivery, even at low temperature and in the presence of metabolic inhibitors (*52*). In our case, CPP allows the QD−CPP conjugates to function as nanoscale vectors for the intracellular delivery of model fluorescent proteins cargos. Further, the conjugates essentially constitute multifunctional platforms, where the nanocrystals provide a fluorophore for visualization and scaffolds for immobilizing proteins and CPP, two biologically active "receptors" with different functions and spatial extensions. As YFP and b-PE are fluorescent, they also provide an additional means for conjugate visualization, and verification of both colocalization and delivered protein cargo integrity. The successful delivery of QD-CPP-YFP/b-PE conjugates into both HEK-293 and COS-1 cell lines proves that assembling additional larger size proteins on the nanocrystal surface does not interfere with the ability of CPP to mediate intracellular uptake of QD assemblies, a result that is *a priori* unexpected. Our results also show that multiple noncovalent conjugation schemes based on metal affinity self-assembly and biotin−avidin binding can be simultaneously applied within the same complex, without requiring further purification, to produce multifunctional QD bioconjugates that are stable even in intracellular environments. We found that the labeled cells displayed similar viability as that noted in our previous study

where little to no cytotoxicity was noted in cells exposed to QD bioconjugates for short 1 h incubations. We have also followed QD−CPP bioconjugates from 3−7 days following uptake and 1−3 days after microinjection with no apparent cytotoxicity noted (data not shown).

Although fluorescent proteins have become ubiquitous in biological research (*53*), there has not been much work aimed at exploiting hybrid dual fluorescent QD−protein conjugates beyond two preliminary studies investigating resonance energy transfer between QDs and fluorescent proteins (*54, 55*). Our study shows the potential of such conjugates to explore specific issues such as intracellular delivery and conjugate distribution inside live cells. The ability of the relatively small cell penetrating peptide to facilitate the intracellular delivery of large protein cargos is rather remarkable. Our data suggest that by utilizing an average of ∼10 YFPs plus a nominal 50 CPP per QD, intracellular delivery of protein cargos with molecular weights of at least ∼300 kDa and a spatial extension of ∼150 Å can be achieved; the size estimate takes into account the nanocrystal and protein/peptide dimensions. The delivered cargos for QD−b-PE conjugates have much larger size and molecular weight. For instance, with an average of 2.5 Streptavidin−b-PE per conjugate, the delivered assemblies have a molecular weight that potentially exceeds $\sim 10^3$ kDa and overall dimensions approaching ∼500 Å. Molecular weight and size can increase quite substantially if conjugates with higher b-PE valences are used.

This study also provides further insight into CPP-mediated capabilities and confirms our earlier findings that nanoparticle conjugates taken up via this method are primarily distributed within endolysosomal compartments (*25*). Although CPP-mediated delivery is an efficient method of intracellular delivery and labeling of many different types of cells, a variety of cellular biosensing and translocation assays will ultimately require cytosolic distribution rather than endosomal confinement of the QD conjugates. Some techniques are available for nucleic acid transfection through endosomes; however, consistent and efficient endosomal escape methodologies, especially for functionalized nanoparticles, have yet to be developed (*56, 57*). As such, cellular microinjection was evaluated as an alternate technique for delivering the QD−FP conjugates. Although a physical technique usually requiring manual operation, cellular microinjection is one of the few methods that can allow direct and consistent access to the cytosol of different cell types (*58*). The same 1:1 540 nm QD−b-PE bioconjugates utilized above, without additional CPP, were microinjected directly into the cytosol of both HEK293/T17 and COS-1 cells. Figure 7 show representative micrographs where the superimposed DIC and fluorescent images demonstrate a well-dispersed conjugate distribution across the entire cytoplasm, as opposed to the more localized and punctuate staining typically observed with CPP-mediated delivery. Though this delivery route is less efficient, since cells must be individually injected, it offers an alternative approach for targeted delivery of controlled cargo materials (such as drugs) directly into the cytoplasm of an array of live cells. This could potentially allow subsequent cellular effects to be intimately studied along with the tracking of other intracellular markers.

In summary, we have shown the remarkable ability of CPP to function as a simple and effective peptidic tool that can facilitate intracellular delivery of luminescent QDs decorated with both small and large protein cargos. Based on the multifunctional architecture demonstrated here, these hybrid nanostructures provide ideal tools for investigating intracellular tracking of proteins, protein−protein interactions, and potentially drug delivery (*2, 8, 9, 59, 60*). Such multifunctional QD conjugates could allow the evaluation of critical issues such as efficiency of cellular uptake, endosomal escape, intracellular conjugate stability, and intracellular fate through the simultaneous monitoring of QD and fluorescent protein emissions. Other recently described strategies aiming to address these questions necessitated multiple, complex synthetic steps to prepare the probe and rely on multiple metabolic processes and inference for results (*61*). Self-assembly of probes with control over their structures and direct monitoring of fluorescent signals potentially offers a much simpler approach. Including additional functionalities in the QD cargo such as FRET-based sensors (*50, 62*), for example, could report on cellular physiology and responses to environmental or drug-induced challenges. Furthermore, substituting or simply adding other targeting peptides within the conjugate could also provide the means to evaluate the delivery efficacy of such cargos to particular cellular organelles. Future experiments will focus on studying QD−fluorescent protein FRET interactions intracellularly as a means of monitoring both conjugate fate and integrity over time. Lastly, it is worth noting that it is exactly these types of multifunctional nanoparticle assemblies that are projected to form the basis of next-generation nanomedicine and diagnostics (*1−5, 8, 9, 59, 60, 63*) and it is clear that semiconductor quantum dots may play an important tole in their development.

ACKNOWLEDGMENT

The authors acknowledge Stephen Lee and Ilya Elashvilli of the CB Directorate/Physical S&T Division (DTRA), ONR, NRL, and the NRL-NSI for financial support. T.P. acknowledges a postdoctoral fellowship from the Fondation pour la Recherche Medicale (France).

LITERATURE CITED

(1) Luccardini, C., Yakovlev, A., Gaillard, S., van't Hoff, M., Alberola, A. P., Mallet, J.-M., Parak, W. J., Feltz, A., and Oheim, M. J. (2007) Getting across the plasma membrane and beyond: Intracellular uses of colloidal semiconductor nanocrystals. *Biomed. Biotechnol.* Article ID 68963.

(2) Ozkan, M. (2004) Quantum dots and other nanoparticles: what can they offer to drug discovery?". *Drug Discovery Today 9*, 1065–1071.

(3) Emerich, D. F., and Thanos, C. G. (2006) The pinpoint promise of nanoparticle-based drug delivery and molecular diagnosis. *Biomol. Eng. 23*, 171–184.

(4) Hilda, W. A., Breuniga, M., and Goepferich, A. (2007) Quantum dots - Nano-sized probes for the exploration of cellular and intracellular targeting. *Eur. J. Pharm. Biopharm. 68*, 153–168.

(5) Sukhorukov, G. B., and Mohwald, H. (2007) Multifunctional cargo systems for biotechnology. *TRENDS Biotechnol. 25*, 93–98.

(6) Medintz, I., Uyeda, H., Goldman, E., and Mattoussi, H. (2005) Quantum dot bioconjugates for imaging, labeling and sensing. *Nat. Mater. 4*, 435–446.

(7) Michalet, X., Pinaud, F. F., Bentolila, L. A., Tsay, J. M., Doose, S., Li, J. J., Sundaresan, G., Wu, A. M., Gambhir, S. S., and Weiss, S. (2005) Quantum dots for live cells, in vivo imaging, and diagnostics. *Science 307*, 538–544.

(8) Azzazy, H. M. E., Mansour, M. M.H., and Kazinierczak, S. C. (2007) From diagnostics to therapy: Prospects of quantum dots. *Clin. Biochem. 40*, 917–927.

(9) Hild, W. A., Breunig, M., and Goepferich, A. (2008) Quantum dots - Nano-sized probes for the exploration of cellular and intracellular targeting. *Eur. J. Pharm. Biopharm. 68*, 153–68.

(10) Pons, T., Uyeda, H. T., Medintz, I. L., and Mattoussi, H. (2006) Hydrodynamic dimensions, electrophoretic mobility and stability of hydrophilic quantum dots. *J. Phys. Chem. B 110*, 20308–20316.

(11) Jaiswal, J. K., Mattoussi, H., Mauro, J. M., and Simon, S. M. (2003) Long-term multiple color imaging of live cells using quantum dot bioconjugates. *Nat. Biotechnol. 21*, 47–51.

(12) Chen, F. Q., and Gerion, D. (2004) Fluorescent CdSe/ZnS nanocrystal-peptide conjugates for long-term, nontoxic imaging and nuclear targeting in living cells. *Nano Lett. 4*, 1827–1832.

(13) Derfus, A. M., Chan, W. C. W., and Bhatia, S. N. (2004) Intracellular delivery of quantum dots for live cell labeling and organelle tracking. *Adv. Mater. 16*, 961–966.

(14) Voura, E., B., Jaiswal, J. K., Mattoussi, H., and Simon S. M. (2004) Tracking early metastatic progression with quantum dots and emission scanning microscopy. *Nat. Med. 10*.

(15) Chan, W. C. W., and Nie, S. (1998) Quantum dot bioconjugates for ultrasensitive nonisotopic Detection. *Science 281*, 2016–2018.

(16) Hoshino, A., Fujioka, K., Oku, T., Nakamura, S., Suga, M., Yamaguchi, Y., Suzuki, K., Yasuhara, M., and Yamamoto, K. (2004) Quantum dots targeted to the assigned organelle in living cells. *Microbiol. Immunol. 48*, 985–994.

(17) Lagerholm, B. C., Weinreb, G. E., Thompson, N. L., and Jacobson, K. (2004) Probing membrane heterogeneity with quantum dots. *Mol. Biol. Cell 15*, 317A.

(18) Rozenzhak, S. M., Kadakia, M. P., Caserta, T. M., Westbrook, T. R., Stone, M. O., and Naik, R. R. (2005) Cellular internalization and targeting of semiconductor quantum dots. *Chem. Commun. 17*, 2217–2219.

(19) Silver, J., and Ou, W. (2005) Photoactivation of quantum dot fluorescence following endocytosis. *Nano Lett. 5*, 1445–1449.

(20) Biju, V., Muraleedharan, D., Nakayama, K., Shinohara, Y., Itoh, T., Baba, Y., and Ishikawa, M. (2007) Quantum dot-insect neuropeptide conjugates for fluorescence imaging, transfection, and nucleus targeting of living cells. *Langmuir 23*, 10254–10261.

(21) Chang, J. C., Su, H. L., and Hsu, S. H. (2007) The use of peptide-delivery to protect human adipose-derived adult stem cells from damage caused by the internalization of quantum dots. *Biomaterials 29*, 925–936.

(22) Lei, Y., Tang, H., Yao, L., Yu, R., Feng, M., and Zou, B. (2008) Applications of mesenchymal stem cells labeled with Tat peptide conjugated quantum dots to cell tracking in mouse body. *Bioconjugate Chem. 19*, 421–427.

(23) Ruan, G., Agrawal, A., Marcus, A. I., and Nie, S. (2007) Imaging and tracking of Tat peptide- conjugated quantum dots in living cells: New insights into nanoparticle uptake, intracellular transport, and vesicle shedding. *J. Am. Chem. Soc. 129*, 14759–14766.

(24) El-Andaloussi, S., Holm, T., and Langel, U. (2005) Cell-penetrating peptides: Mechanisms and applications. *Curr. Pharm. Des. 11*, 3597–3611.

(25) Delehanty, J. B., Medintz, I. L., Pons, T., Brunel, F. M., Dawson, P. E., and Mattoussi, H. (2006) Self-assembled quantum dot-peptide bioconjugates for selective intracellular delivery. *Bioconjugate Chem. 17*, 920–927.

(26) Sapsford, K. E., Pons, T., Medintz, I. L., Higashiya, S., Brunel, F. M., Dawson, P. E., and Mattoussi, H. (2007) Kinetics of metal-affinity driven self-assembly between proteins or peptides and CdSe-ZnS quantum dots. *J. Phys. Chem. C 111*, 11528–11538.

(27) Clapp, A. R., Pons, T., Medintz, I. L., Delehanty, J. B., Melinger, J. S., Tiefenbrunn, T., Dawson, P. E., Fisher, B. R., O'Rourke, B., and Mattoussi, H. (2007) Two-photon excitation of quantum dot-based fluorescence resonance energy transfer and its applications. *Adv. Mater. 119*, 1921–1926.

(28) Murray, C. B., Norris, D. J., and Bawendi, M. G. (1993) Synthesis and characterization of nearly monodisperse CdE (*E* = sulfur, selenium, tellurium) semiconductor nanocrystallites. *J. Am. Chem. Soc. 115*, 8706–15.

(29) Qu, L., Peng, Z. A., and Peng, X. (2001) Alternative routes toward high quality CdSe nanocrystals. *Nano Lett. 1*, 333–337.

(30) Dabbousi, B. O., Rodriguez-Viejo, J., Mikulec, F. V., Heine, J. R., Mattoussi, H., Ober, R., Jensen, K. F., and Bawendi, M. G. (1997) (CdSe)ZnS core-shell quantum dots: synthesis and optical and structural characterization of a size series of highly luminescent materials. *J. Phys. Chem. B 101*, 9463–9475.

(31) Clapp, A. R., Goldman, E. R., and Mattoussi, H. (2006) Capping of CdSe-ZnS quantum dots with DHLA and subsequent conjugation with proteins. *Nat. Protocols 1*, 1258–66.

(32) Mattoussi, H., Mauro, J. M., Goldman, E. R., Anderson, G. P., Sundar, V. C., Mikulec, F. V., and Bawendi, M. G. (2000) Self-assembly of CdSe-ZnS quantum dot bioconjugates using an engineered recombinant protein. *J. Am. Chem. Soc. 122*, 12142–12150.

(33) Uyeda, H. T., Medintz, I. L., Jaiswal, J. K., Simon, S. M., and Mattoussi, H. (2005) Synthesis of compact multidentate ligands to prepare stable hydrophilic quantum dot fluorophores. *J. Am. Chem. Soc. 127*, 3870–3878.

(34) Susumu, K., Uyeda, H. T., Medintz, I. L., Pons, T., Delehanty, J. B., and Mattoussi, H. (2007) Enhancing the stability and biological functionalities of quantum dots via compact multifunctional ligands. *J. Am. Chem. Soc. 129*, 13987–96.

(35) Deuschle, K., Okumoto, S., Fehr, M., Looger, L. L., Kozhukh, L., and Frommer, W. B. (2005) Construction and optimization of a family of genetically encoded metabolite sensors by semirational protein engineering. *Protein Sci. 14*, 2304–2314.

(36) Medintz, I. L., Goldman, E. R., Lassman, M. E., and Mauro, J. M. (2003) A fluorescence resonance energy transfer sensor based on maltose binding protein. *Bioconjugate Chem. 14*, 909–918.

(37) Minaschek, G., Bereiterhahn, J., and Bertholdt, G. (1989) Quantitation of the volume of liquid injected into cells by means of pressure. *Exp. Cell Res. 183*, 434–442.

(38) Tsien, R. Y. (1998) The green fluorescent protein. *Annu. Rev. Biochem. 67*, 509–544.

(39) Nguyen, A. W., and Daugherty, P. S. (2005) Evolutionary optimization of fluorescent proteins for intracellular FRET. *Nat. Biotechnol. 23*, 355–360.

(40) Schmid, J. A., and Neumeier, H. (2005) Evolutions in science triggered by green fluorescent protein (GFP). *ChemBioChem 6*, 1149–1156.

(41) Shaner, N. C., Campbell, R. E., Steinbach, P. A., Giepmans, B. N. G., Palmer, A. E., and Tsien, R. Y. (2004) Improved monomeric red, orange and yellow fluorescent proteins derived from *Discosoma* sp red fluorescent protein. *Nat. Biotechnol. 22*, 1567–1572.

(42) Glazer, A. N. (1985) Light harvesting by phycobilisomes. *Annu. Rev. Biophys. Biophys. Chem. 14*, 47–77.

(43) Glazer, A. N. (1994) Phycobiliproteins - a family of valuable, widely used fluorophores. *J. Appl. Phycol. 6*, 105–112.

(44) Sandros, M. G., Gao, D., and Benson, D. E. (2005) A modular nanoparticle-based system for reagentless small molecule biosensing. *J. Am. Chem. Soc. 127*, 12198–12199.

(45) Ipe, B. I., Shukla, A., Lu, H., Zou, B., Rehage, H., and Niemeyer, C. M. (2006) Dynamic light- scattering analysis of the electrostatic interaction of hexahistidine-tagged cytochrome P450 enzyme with semiconductor quantum dots. *ChemPhysChem 7*, 1112–1118.

(46) Liu, W., Howarth, M., Greytak, A. B., Zheng, Y., Nocera, D. G., Ting, A. Y., and Bawendi, M. G. (2008) Compact biocompatible quantum dots functionalized for cellular imaging. *J. Am. Chem. Soc. 130*, 1274–84.

(47) Hermanson, G. T. (1996) *Bioconjugate Techniques*, Academic Press, San Diego.

(48) Pons, T., Medintz, I. L., Wang, X., English, D. S., and Mattoussi, H. (2006) Solution-phase single quantum dot fluorescence resonant energy transfer sensing. *J. Am. Chem. Soc. 128*, 15324–15331.

(49) Clapp, A. R., Medintz, I. L., Mauro, J. M., Fisher, B. R., Bawendi, M. G., and Mattoussi, H. (2004) Fluorescence resonance energy transfer between quantum dot donors and dye-labeled protein acceptors. *J. Am. Chem. Soc. 126*, 301–310.

(50) Medintz, I. L., Clapp, A. R., Brunel, F. M., Tiefenbrunn, T., Uyeda, H. T., Chang, E. L., Deschamps, J. R., Dawson, P. E.,

and Mattoussi, H. (2006) Proteolytic activity monitored by fluorescence resonance energy transfer through quantum-dot-peptide conjugates. *Nat. Mater. 5*, 581–589.
(51) Wu, X., Liu, H., Liu, J., Haley, K. N., Treadway, J. A., Larson, J. P., Ge, N., Peale, F., and Bruchez, M. P. (2003) Immunofluorescent labeling of cancer marker Her2 and other cellular targets with semiconductor quantum dots. *Nat. Biotechnol. 21*, 41–46.
(52) Torchilin, V. P., Rammohan, R., Weissig, V., and Levchenko, T. S. (2001) TAT peptide on the surface of liposomes affords their efficient intracellular delivery even at low temperature and in the presence of metabolic inhibitors. *Proc. Natl. Acad. Sci. U.S.A. 98*, 8786–8791.
(53) Shaner, N. C., Steinbach, P. A., and Tsien, R. Y. (2005) A guide to choosing fluorescent proteins. *Nat. Methods 2*, 905–909.
(54) Geissbuehler, I., Hovius, R., Martinez, K. L., Adrian, M., Thampi, K. R., and Vogel, H. (2005) Lipid-coated nanocrystals as multifunctionalized luminescent scaffolds for supramolecular biological assemblies. *Angew. Chem., Int. Ed. 44*, 1388–1392.
(55) Hering, V. R., Gibson, G., Schumacher, R. I., Faljoni-Alario, A., and Politi, M. J. (2007) Energy transfer between CdSe/ZnS Core/Shell quantum dots and fluorescent proteins. *Bioconjugate Chem. 18*, 1705–1708.
(56) Yessine, M. A., and Leroux, J. C. (2004) Membrane-destabilizing polyanions:interaction with lipid bilayers and endosomal escape of biomacromolecules. *Adv. Drug Delivery Rev. 56*, 999–1021.
(57) Luo, D. (2005) Nanotechnology and DNA delivery. *MRS Bull. 30*, 654–658.
(58) Petit, A. C., Legue, E., and Nicolas, J. F. (2005) Methods in clonal analysis and applications. *Reprod. Nutr. Dev. 45*, 321–339.
(59) Sukhorukov, G. B., Rogach, A. L., Zebli, B., Liedl, T., Skirtach, A. G., Kohler, K., Antipov, A. A., Gaponik, N., Susha, A. S., Winterhalter, M., and Parak, W. J. (2005) Nanoengineered polymer capsules: Tools for detection, controlled delivery, and site-specific manipulation. *Small 1*, 194–200.
(60) Conti, M., Tazzari, V., Baccini, C., Pertici, G., Serino, L. P., and De Giorgi, U. (2006) Anticancer drug delivery with nanoparticles. *In Vivo 20*, 697–701.
(61) Lee, Y. J., Datta, S., and Pellois, J. P. (2008) Real-time fluorescence detection of protein transduction into live cells. *J. Am. Chem. Soc. 130*, 2398–2399.
(62) Medintz, I. L., Clapp, A. R., Mattoussi, H., Goldman, E. R., Fisher, B., and Mauro, J. M. (2003) Self-assembled nanoscale biosensors based on quantum dot FRET donors. *Nat. Mater. 2*, 630–638.
(63) Bakalova, R., Zhelev, Z., Aoki, I., and Kanno, I. (2007) Designing quantum-dot probes. *Nat. Photon. 1*, 487–489.

BC800089R